engineering proceedings

MDPI

Proceeding Paper

Enhancing Voltage and Power Output Through Structural Optimization of Coil-Magnet Transducers in Electromagnetic Vibration Energy Harvesters †

Tunde Isaiah Toluwaloju and Chung Ket Thein *

Department of Mechanical, Materials and Manufacturing Engineering, University of Nottingham Ningbo China, Ningbo 315100, China; Tunde.TOLUWALOJU@nottingham.edu.cn

* Correspondence: chungket.thein@nottingham.edu.cn

† Presented at The 11th International Electronic Conference on Sensors and Applications (ECSA-11), 26–28 November 2024; Available online: https://sciforum.net/event/ecsa-11.

Abstract: Electromagnetic vibration energy harvesters (EVEHs) has emerged as a promising approach to power small electronic devices and sensors, particularly in remote or inaccessible locations where traditional power sources are impractical. This study investigates approaches for structurally scaling and optimizing the EVEH transducer magnet structure to maximize the magnet flux density, total flux density, harvested voltages and power output. Six design configurations have been analyzed in different coils and transducer magnet/flux guiding steel geometries. While the coil are varies by using bulk or split coils, the magnet/flux guiding steel are varied by using different sizes. Analytical validation and simulations showed that these variations generally affected the transducer flux density per unit magnet volume $\left(\beta_{V_{mag}}\right)$ and total volume $\left(\beta_{V_{Tot}}\right)$. Validation shows that configurations with split center magnet with the smallest transducer volume attains preferable $\beta_{V_{mag}}, \beta_{V_{Tot}}$ and power density by approximately 21.66%, 15.77% and 54.47% over reference model without center magnet/steel. Therefore, the most structurally optimized configuration attained lightweight but yet higher energy conversion/flux coupling efficiency. Also, analysis showed using split slotted coils are more efficient for energy harvesting than bulk equivalent (single) coils counterparts. This is because the split coil will encourage much flux coupling than bulk coil. Additionally, the optimal load capacity is considerable reduce by approximately 50.00% on configurations with split coil. Therefore, split and bulk are respectively suitable for low and high impedance matching.

Keywords: electromagnetic vibration energy harvester; magnet arrangement; transducers; sustainable energy

Citation: Toluwaloju, T.I.; Thein, C.K. Enhancing Voltage and Power Output Through Structural Optimization of Coil-Magnet Transducers in Electromagnetic Vibration Energy Harvesters. *Eng. Proc.* **2024**, *6*, x. https://doi.org/10.3390/xxxxx

Academic Editor(s): Name

Published: 26 November 2024

1. Introduction

Vibration energy harvesting has emerged as an effective approach to power small electronic devices and sensors, particularly in remote or inaccessible locations where traditional power sources are impractical [1]. Among the various transducer mechanisms, electromagnetic vibration energy harvesters (EVEHs) have garnered significant attention due to their relatively simple design, high energy conversion efficiency, and scalability [2,3]. Generally, the performance of EVEHs is heavily dependent on the structural configuration and relative positioning of the magnets and coils within the transducer [4,5]. Numerous studies have investigated strategies to optimize the EVEH design and enhance its power output. Saha et al. [6] analyzed the effect of magnet-coil gap on the voltage and power generation and reported an optimal gap distance for maximum performance. Similarly, Zhu et al. [7] explored the influence of coil position and found that an off-center coil configuration can improve the EVEH's power density. In addition to the magnet-coil

arrangement, the magnetic flux density within the transducer also plays a crucial role in determining the EVEH's performance [8,9]. Researchers have proposed various techniques to optimize the magnetic circuit, such as utilizing Halbach arrays [10] or incorporating flux-concentrating elements [11], to maximize the magnetic flux linkage and, consequently, the harvested power. Recent advancements in computational modeling and simulation have enabled more comprehensive optimization of EVEH structures. Analytical models have been developed to predict the open-circuit voltage and power output, which are then validated through experimental measurements on prototype systems [12,13]. These models provide a powerful tool for exploring the design space and identifying optimal configurations that can significantly enhance the EVEH's performance. Several studies have demonstrated the effectiveness of structural optimization in improving the voltage and power output of EVEHs. Tao et al. [14] reported a 35% increase in power output by optimizing the magnet and coil positions. Deng et al. [15] introduced a multi-magnet EVEH design that achieved a 40% improvement in power density compared to a single-magnet configuration. Similarly, Xie et al. [16] proposed a segmented magnet arrangement that enhanced the EVEH's power output by up to 50%. The continued research and development in this field have led to the emergence of various advanced EVEH designs, such as those incorporating magnetic levitation [17], flux feedback mechanisms in the harvester magnet transducer [18], and hybrid transducer mechanisms [19]. These innovations aim to further improve the energy harvesting capabilities and expand the applicability of EVEHs in powering a wide range of self-powered and sustainable electronics.

In summary, the optimization of EVEH structures by strategically positioning the magnets and coils has been a major focus of research in recent years. The literature demonstrates that significant improvements in the harvested voltages and power can be achieved through comprehensive parametric analysis and optimization. The findings from these studies provide valuable insights for the design and implementation of high-performance EVEHs, contributing to the advancement of self-powered and sustainable electronic systems.

2. Governing Equation of a Spring-Mass Model

To effectively generalize the equation that governs the electromagnetic vibration energy harvester (EVEH) whose transducer coil-magnet properties are to be structurally optimized for improved performances, the EVEH is shows as a spring-mass model as shown in Figure 1. The general equation that governs the responses of the model in Figure 1 is shown in Equation (1)

$$\mathrm{m}_e\ddot{Y}(t) + 2\mathrm{m}_e\zeta_{eq}\omega_n\dot{Y}(t) + kY(t) + F_r\mathrm{sgn}\left(\dot{Y}\right) = \mathrm{m}_e\omega^2 Fcos(\omega t + \varphi) \quad (1)$$

From Figure 1, $\mathrm{m}_e, k, \omega, \omega_n, \zeta_{eq}, F, \varphi, F_r$ and $Y(t)$ are the model effective mass, linear stiffness, excitation frequency, resonance frequency, total damping ratio in the system, excitation amplitude, phase shift between the excitation and the mass displacement, Coulomb friction force in the system and the response amplitude in the temporal coordinates. The total damping ratio in the system (ζ_{eq}) is defined as the linear summation of the damping contributions from the mechanical (ζ_m) and electromagnetic (ζ_{em}) loss components.

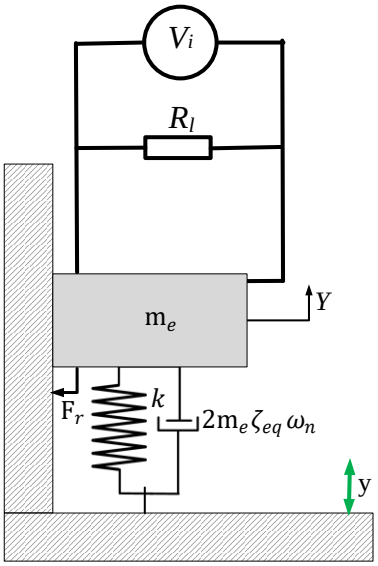

Figure 1. Spring mass model of the EVEH.

This study investigates how the EVEH magnet structure could maximize the flux densities per magnet volume, harvested voltages and power output by a comparatively study using three (3) design scenarios. When vibration is induced in the spring-mass model of Figure 1, the mass (magnet) mounted on the spring will oscillate, therefore voltage will be induced in the transducer coil as it cuts through the fields of the spring mounted permanent magnets or vice versa. As the coil interact with the permanent magnet field in a steady and continuous periodic motion, voltage is induced. The induced voltage are computed using the Faraday principle of electromagnetic induction. The steady state relative and absolute amplitude solution of the spring-mass (coil) model for each i^{th} configurations are obtained as shown in Equations (2) and (3) $\forall\, i = a, b$ and c

$$Y_i = -G_i \frac{F_{r_i}}{K} + F\sqrt{{Q_i}^2 r_i^4 - \left(\frac{H_i F_{r_i}}{K}\right)^2} \tag{2}$$

$$X_i = \sqrt{\mathrm{Y}_i^2 + F_0^2 + 2F_0 Y_i \cos\varphi_i} \tag{3}$$

where k is the spring stiffness, r is the frequency ratio, other parameters in Equations (2) and (3) are listed in the appendix section is defined as shown in Appendix A. Likewise, the total damping ratio (ζ_{eq_i}) components for each i^{th} transducer configuration is shown in Equations (4) and (5) where c_{m_i} is the springs mechanical damping constant.

$$\zeta_{m_i} = \frac{c_{m_i}}{2\mathrm{m}_{e_i}\omega_i} \tag{4}$$

$$\zeta_{em_i} = \frac{8\mathrm{K}_i^2 {l_{c_i}}^2}{2\mathrm{m}_{e_i}\omega_i}\left(\frac{1}{R_{l_i} + R_{c_i}}\right) \tag{5}$$

$$K_i = N_i b_i C_{f_i} l_{c_i} \tag{6}$$

To complete a close circuit for voltage/power harvesting, the harvester model it is required that the harvester model is connected over an external load resistor as shown in Figure 1. When the transducer coil with internal resistance (R_{c_i}) is connected over an external load having a resistance (R_{l_i}), for each i^{th} configuration, N_i, b_i, C_{f_i}, and l_{c_i} are transducer coil turn number, coupling coefficient, external load resistance, internal resistance of the coil, and effective coil length. The coupling coefficient K_i is defined as the

number of the flux line that cuts the coil is defined as shown in Equation (6). The average flux density induced in the regions of the i^{th} coil was simulated on the Finite Element Magnetic Method (FEMM) software as shown in Figures 2, 3 and 4. Also, the expression for the harvester voltage and power harvested over the R_l for each i^{th} configurations are obtained as shown in Equations (7) and (8) respectively $\forall\, i = a, b,$ and c.

$$V_i = 4K_i l_{c_i} Y_i \omega_i \left(\frac{R_{l_i}}{R_{l_i} + R_{c_i}} \right) \tag{7}$$

$$P_i = 16K_i^2 {l_{c_i}}^2 Y_i^2 \omega_i^2 \frac{R_{l_i}}{\left(R_{l_i} + R_{c_i}\right)^2} \tag{8}$$

The determination of the model's optimal load was achieved using the maximum power transfer theorem, which stipulates that the rate of change of output power with respect to load resistance $\frac{\delta P_{Out}}{\delta R_l} = 0$. This derivative yields an expression for the optimal load resistance $\left(R_l^{opt}\right)$, as indicated in Equation (9), where c_i represent the mechanical damping coefficient.

$$R_l^{opt} = \frac{16K_i^2 l_{c_i}^2}{c_{m_i}} + R_{c_i} \tag{9}$$

3. Transducer Coil-Magnet Models

To investigate different optimization strategies for the coil-magnet transducer geometries, the design models 'a', 'b' and 'c' analyzed are shown in Figure 2.

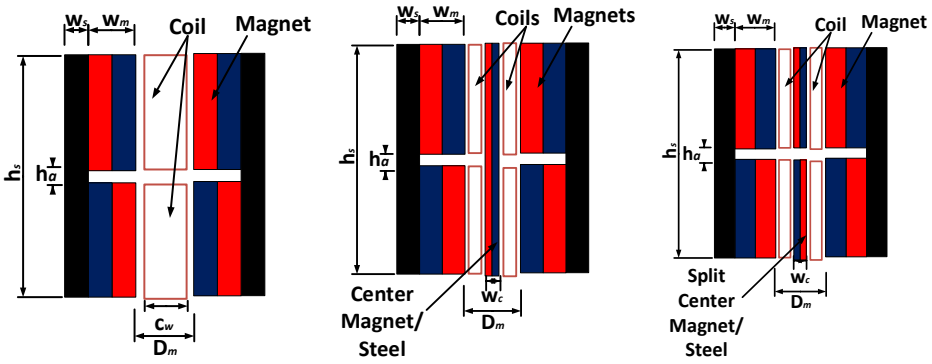

Figure 2. Configuration a; transducer coil-magnet models; single slotted coil-four magnets circuit (**left**), Configuration b; double slotted coils-split magnet circuit with conductive steel in the center (**middle**) and Configuration c; double slotted coils with split conductive magnet/steel in the center (**right**).

In the following analysis, each of the model is referred to configurations a, b, and c respectively where configuration 'a' is the reference. From Figure 2, h_s, h_a and h_m are the heights of the flux guiding steel, transducer magnet/coils air gap, and transducer magnets. Also c_w, w_m, w_c and w_s are coil width, width of the transducer magnets, width of the center circuit splitting material (magnet/iron) and width of the flux guiding steel respectively. For simplicity and effective comparison of the respective designs, the minimum clearance distance which ensures that there is not dynamic contact between the coil and the magnet during dynamic operation is fixated at $c_d = 0.875$ mm and h_a is also fixed at 2.00 mm for all. From Figure 2, configuration 'a' is the reference model using a bulk no split coil. Also, configuration b1 and b2 uses a continuous steel and magnet material at the center respectively to achieve a split coil slots with flux guiding steel. However, to maximize the structural geometrical variations in the configurations 'c', itis further simplified into a total of three (3) design variations 'c1', 'c2' and 'c3'. Configurations 'c1',

and 'c2' are respectively defined as using a split steel and magnet material at the center to achieve a split coil slots without outer flux guiding steel while 'c3' is using a split magnet material at the center to achieve a split coil slots with outer flux guiding steel. The respective values of h_s, h_m, c_w, w_m and w_s for the design configuration 'a', 'b1', 'b2', 'c1', 'c2' and 'c3' is shown in Table 1.

Table 1. Summary of magnet dimensions for transducer models 1, 2, and 3.

Configuration	i	h_s(mm)	h_a(mm)	h_m(mm)	c_w(mm)	w_m(mm)	w_s(mm)	w_c(mm)
a	1	22.00	2.00	10.00	8.00	5.00	5.00	0.00
b	1	22.00	2.00	10.00	4.00	5.00	5.00	2.50
	2	22.00	2.00	10.00	4.00	5.00	5.00	2.50
c	1	22.00	2.00	10.00	4.00	5.00	0.00	2.50
	2	22.00	2.00	10.00	4.00	2.50	0.00	2.50
	3	22.00	2.00	10.00	4.00	2.50	2.50	2.50

For each configurations, the effective total volume (V_{Tot}) and effective magnet volume (V_m) are computed. While V_{Tot} represents the total volume of the transducer model, V_m is defined as the total magnet volume in the model designs. Likewise, when the flux density in the area occupied by the transduction coil is measured as b, the flux density per total volume $(\beta_{V_{Tot}})$ and the flux density per magnet volume (β_{mag}) was computed as the parameter for quantify the design parameters.

4. Finite Element Magnetic Method (FEMM) Simulation

This section clearly reports the method for quantifying the fluxed within the coil region in the transducer geometry in brief. The respective FEMM results for the different geometry is shown in Figures 3 and 4.

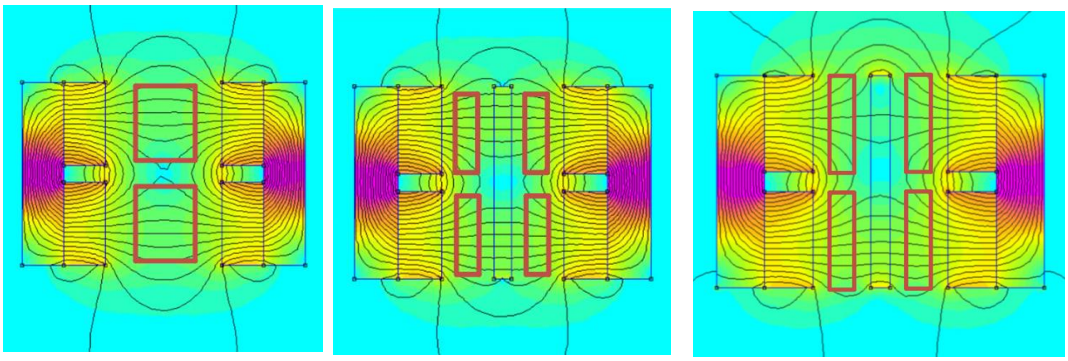

Figure 3. FEMM simulation configurations a (**left**), b1 and (**middle**), and b2 (**right**).

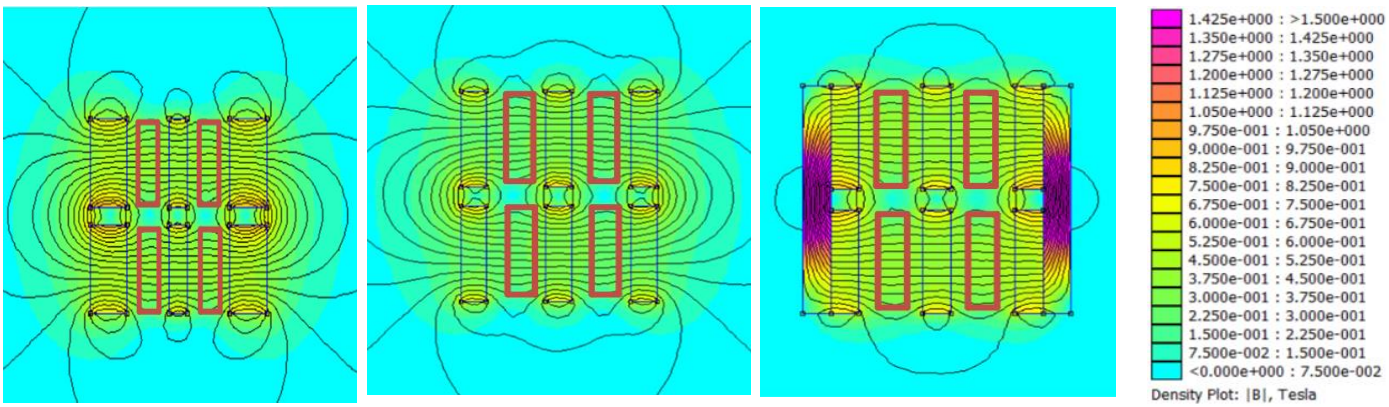

Figure 4. FEMM simulation configurations c1 (**left**), c2 (**middle**) and c3 (**right**).

In Figures 3 and 4, the red highlight portion are used to define the location of the coil in static equilibrium. During dynamic operation (energy harvesting), the coil begins to oscillate in the field of the permanent magnet. This to for oscillation therefore resulted in voltages been induced in the coil.

The respective values of the flux densities in the region where the coil oscillate during energy harvesting are measured and recorded in Table 2.

Table 2. Summary of magnetic flux densities, $V_{mag}, V_{Tot}, \beta_{mag}$, and $\beta_{V_{Tot}}$ for models 1, 2, and 3.

Config.	$\mathbf{D_m}$ $(\mathbf{mm})$	b (T)	$\mathbf{V_{mag}} \times 10^{-5}\ (\mathbf{m^3})$	$\mathbf{V_{Tot}} \times 10^{-5}\ (\mathbf{m^3})$	$\boldsymbol{\beta}_{\mathbf{mag}} \times 10^{4}\ (\mathbf{Tm^{-3}})$	$\boldsymbol{\beta}_{\mathbf{V_{Tot}}} \times 10^{4}\ (\mathbf{Tm^{-3}})$
a1	9.750	0.382	0.5000	1.6362	7.6458	2.3364
b1	14.000	0.332	0.5000	1.8700	6.6718	1.7890
b2	14.000	0.244	0.6250	1.8700	5.9611	1.9923
c1	14.000	0.343	0.6250	1.3200	5.4931	2.6092
c2	14.000	0.251	0.3750	1.0450	6.6950	2.4025
c3	14.000	0.368	0.3750	1.3200	9.7598	2.7737

5. Results and Parametric Analysis

This section investigated and quantified how the structural optimization of coil-magnet transducer shown in Figure 2 enhanced or compromised the spring-mass EVEH voltage and power output. To complete a close circuit for voltage/power harvesting, the harvester model it is required that the harvester model is connected over an external load resistor as shown in Figure 1. The respective equations for computing the harvested voltages and power are given in Equations (7) and (8) while Equation (9) shows the value of the resistance at which the external load becomes optimized. This stage of analysis shall be undertaken in two stages. The first stages shall focus on characterizing which design configuration is most proficient for application in term of b, β_{mag} and $\beta_{V_{Tot}}$. Using the appropriate power equation, the second stage of analysis shall investigate the relative harvestable power/voltage performances. Finally, the conclusion part of this report will identify the relevant performance preference as a consequences of the initial stages of analysis.

A. b, β_{mag} and $\beta_{V_{Tot}}$ variation: This stage of analysis briefly illustrate the variations of b, β_{mag} and $\beta_{V_{Tot}}$ as a function of the transducer geometrical volume. The flux density per unit volume of the transducer are independently compare as a ratio of total volume and magnet volumes as shown in Table 2. Table 2 show that although configuration a1 has the largest b, β_{mag} for configuration c3 is improved by approximately 21.66%, 31.64%, 38.92%, 43.72% and 31.40% respectively relative to configurations a1, b1, b2, c1 and c2. Also, the $\beta_{V_{Tot}}$ for configuration c3 is improved by 15.77%, 13.39%, 28.17%, 5.93% and 13.38% respectively relative to configurations a1, b1, b2, c1 and c2. Therefore, configuration c3 was identified to attain this preferential density values at the smallest magnet and total volume of 0.3750×10^{-5} m^3 and 1.3200×10^{-5} m^3 compare to other. This suggests that c3 is good enough to represent the improvement in the β_{mag} by approximately 30.00% over other configurations. As shown in the next section, this improvement will definitely result in efficient utilizing of the available magnet flux/magnet volume to induce and enhance the operational efficiency of the system.

B. V_i and P_i variation: This stage of analysis briefly illustrated the variations of the harvested voltages and power as a function of different electrical parameters. Using configuration 1 which has an 8 mm coil width as the reference, configurations 2, 3, 4, 5, and 6 however uses two split 4 mm in the double slot sections of the transducer. To characterize this variation, the coil in each slot points are connected to external load resistances as shown in Figure 5.

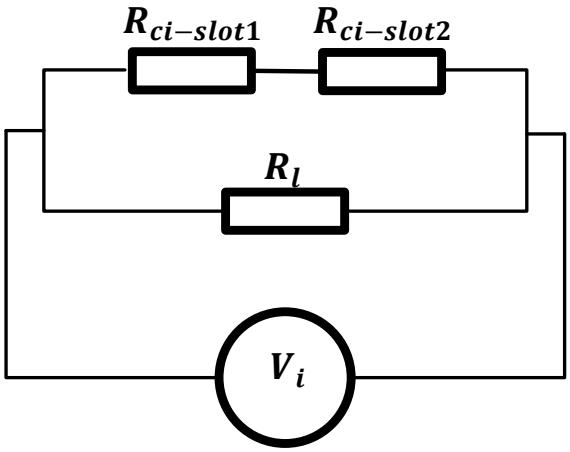

Figure 5. Generalized closed circuit connection of the VEH.

In the eventuality for configuration 1 having only 1 slot coil, Figure 5 reduces by eliminating coil slot 2 and corresponding electrical parameters. The analytical formulations in the above procedure demands that the cumulated power performance comparison for each model is accurately comparable by lump summing the voltage and power on the series connected split coils shown in Figure 5 for configurations 2 to 6 according to Ohms law. The Ohms law asserts that when two voltage sources are connected in series, the effective voltage is the summation of the respective voltage in each sources. Using the Ohms condition, therefore the effective resistances on each coil is therefore obtained as shown in Equation (10).

$$R_T = R_{ci_{slot\,1}} + R_{ci_{slot\,2}} + R_l \tag{10}$$

Using Equation (9), Figure 6(left) and Figure 6(right) shows that the power becomes maximized at optimal resistance values of 48.30 Ω, 22.00 Ω, 18.80 Ω, 23.00 Ω, 19.30 Ω and 24.40 Ω respectively on each slotted coils of 1 to 6.

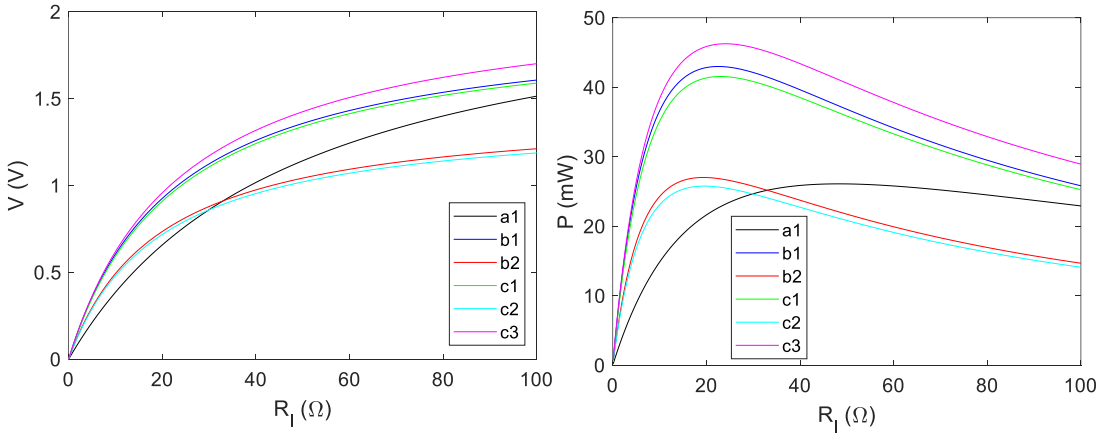

Figure 6. Harvested voltage (**left**) and power (**right**) versus R_l.

The effective coil length $l_c = 2\pi r_e$ where r_e is the effective coil radius, $l_c = 72.571$ mm for configurations 1 to 6. Relevant coil parameter for each slotted coil in each configuration is show in Table 3 where the coil turn for each split coil is 500.

Table 3. Summary of optimum parameter for transducer models.

Config.	a1	b1	b2	c1	c2	c3
$R_{l_i}^{opt}$ (Ω)	48.300	22.000	18.800	23.000	19.300	24.400

P_i^{opt}(mW)	26.102	42.980	27.012	41.543	25.774	46.255

Where r is the frequency ratio of the system, Figure 7 shows the variation of the harvested voltage and power at optimum. Comparing Figure 7, Tables 2 and 3 shows that although configuration 1 (8 mm) attains the highest possible flux density, the optimum characteristics however showed that it optimum harvested resonant power is compromised by approximately 43.57%, 37.17%, 3.37% and 39.69% relative to configurations c3, c1, b2 and b1 respectively. Conversely, the resonant optimum output of a1 is preferable by 12.57% over c2.

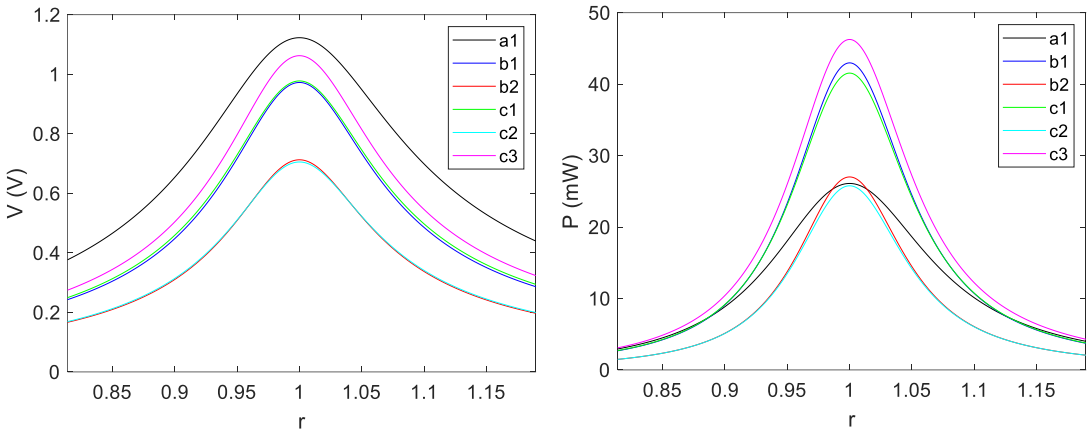

Figure 7. Harvested voltage (**left**) and power (**right**) at $R_{l_i}^{opt}$.

Therefore, Figure 7 establish a generalized trend to quantifying the power variation of the different configuration. Figure 7. Further highlight the observation made in the section where b, β_{mag} and $\beta_{V_{Tot}}$ variation was undertaken. Configuration c3 was identified to efficiently utilize the available magnet volume to induce and enhance the operational efficiency of the system by harvesting highest possible power at equivalent excitation and optimal load comparisons.

6. Conclusions

The following conclusions are reached in this work:

i. A transducer model configuration with smallest volume (c3) attained the highest possible flux density per transducer magnet volume was attained.

ii. Although, flux guiding steel which minimizes flux leakages are often required to enhance flux coupling, configuration c2 which has no such guiding steel likes shows a satisfactory performance next to c3 in term of flux density per unit magnet/total volume, optimum load, harvested voltages and power. The implication of this is that smaller volume lightweight but yet efficient energy conversion/flux coupling are attainable in c3.

iii. Analysis showed using split slotted coils are more efficient for energy harvesting than bulk single equivalent coils. This is because the split coil will encourage much flux coupling/field interaction with the coil, than bulk coil.

iv. The implication of the above implies that while larger power is available for harvesting over a series connected split coil than the bulk coil, the optimal load capacity is considerable reduce by approximately 50.00%. Therefore, for efficient energy conversion and maximized power applicability, the series connected split coils boast of usability for low impedance system, while bulk coil are suitable for high impedance matching.

Author Contributions: Conceptualization, C.K.T.; methodology, C.K.T., T.I.T.; software, T.I.T.; validation, T.I.T.; formal analysis, T.I.T.; investigation, T.I.T.; resources, C.K.T.; data curation, C.K.T.; writing—original draft preparation, T.I.T.; writing—review and editing, C.K.T.; visualization, T.I.T.; supervision, C.K.T.; project administration, C.K.T. All authors have read and agreed to the published version of the manuscript.

Funding: Not applicable.

Institutional Review Board Statement: Not applicable.

Informed Consent Statement: Not applicable.

Data Availability Statement: Data are contained within the article.

Acknowledgments: Not applicable.

Conflicts of Interest: The authors declare no conflict of interest.

Appendix A

$$r_i = \frac{w}{w_{n_i}}, \tau_i = \frac{\pi\sqrt{\zeta_{eq_i}^2 + 1}}{r_i}, \lambda_i = \frac{\pi\zeta_{eq_i}}{r_i}, G_i = \frac{\sinh(\lambda_i) - \frac{\zeta_{eq_i}}{\sqrt{1-\zeta_{eq_i}^2}}\sin(\tau_i)}{\cosh(\lambda_i) + \cos(\tau_i)}$$

$$H_i = \frac{1}{r_i\sqrt{1-\zeta_{eq_i}^2}}\left[\frac{\frac{\zeta_{eq_i}}{\sqrt{1-\zeta_{eq_i}^2}}\sin(\tau_i)}{\cosh(\lambda_i) + \cos(\tau_i)}\right], Q_i = \left[\frac{1}{(\omega_{n_i}^2 - \omega^2)^2 + \left(2\zeta_{eq_i}w_{n_i}\right)^2}\right]^{\frac{1}{2}}$$

$$\varphi_i = tan^{-1}\left[\frac{2\zeta_{eq_i}r_i}{1-r_i^2}\right], w_{n_i} = \sqrt{\frac{k}{m_{e_i}}}$$

where Q_i, G_i and H_i are regarded as the viscous and the transfer functions.

References

1. Priya, S.; Inman, D.J. *Energy Harvesting Technologies*; Springer: Berlin/Heidelberg, Germany, 2009.
2. Beeby, S.P.; Tudor, M.J.; White, N.M. Energy harvesting vibration sources for microsystems applications. *Meas. Sci. Technol.* **2006**, *17*, R175–R195.
3. Mitcheson, P.D.; Yeatman, E.M.; Rao, G.K.; Holmes, A.S.; Green, T.C. Energy Harvesting From Human and Machine Motion for Wireless Electronic Devices. *Proc. IEEE* **2008**, *96*, 1457–1486.
4. Elvin, N.G.; Erturk, A.A. *Advances in Energy Harvesting Methods*; Springer: Berlin/Heidelberg, Germany, 2013.
5. Toluwaloju, T.I.; Thein, C.K.; Halim, D. A parametric analysis on performance dependence of electromagnetic vibration harvester on the coil position, coil connection, and magnetic flux density. In Proceedings of the 2022 International Conference on Electrical, Computer, Communications and Mechatronics Engineering (ICECCME), Maldives, 16–18 November 2022; pp. 1–6.
6. Saha, C.R.; O'Donnell, T.; Wang, N.; McCloskey, P. Electromagnetic generator for harvesting energy from human motion. *Sens. Actuators A Phys.* 2008, *147*, 248–253.
7. Zhu, D.; Roberts, S.; Tudor, M.J.; Beeby, S.P. Design and experimental characterization of a tunable vibration-based electromagnetic micro-generator. *Sens. Actuators A Phys.* 2010, *158*, 284–293.
8. Shu, Y.; Lien, I.; Wu, W. An improved analysis of the performance of a piezoelectric energy harvester. *Smart Mater. Struct.* 2007, *16*, 2253–2264.
9. Toluwaloju, T.I.; Yadav, D.; Thein, C.K.; Halim, D. Investigation on the effect of magnetic coupling and power harvested in an electromagnetic vibration energy harvester. In Proceedings of the 2022 IEEE International Conference on Industrial Technology (ICIT), Shanghai, China, 22–25 August 2022; pp. 1–6.
10. Zhu, D.; Beeby, S.P.; Tudor, M.J.; Harris, N.R. Electromagnetic Vibration Energy Harvesting using an Improved Halbach Array. *Smart Mater. Struct.* **2012**, *20*, 022001.
11. Priya, S. Advances in energy harvesting using low profile piezoelectric transducers. *J. Electroceramics* **2007**, *19*, 165–182.
12. Adhikari, S.; Friswell, M.I.; Inman, D.J. Piezoelectric energy harvesting from broadband random vibrations. *Smart Mater. Struct.* **2009**, *18*, 115005.

13. Foong, F.M.; Thein, C.K.; Yurchenko, D. A two-stage electromagnetic coupling and structural optimization for vibration energy harvesters. *Smart Mater. Struct.* **2020**, *29*, 085002.
14. Tao, K.; Tang, L.; Wu, J.; Lye, S.W.; Chang, H.; Miao, J. Investigation of multimodal electret-based MEMS energy harvester with impact-induced nonlinearity. *J. Microelectromechanical Syst.* **2018**, *27*, 276–288.
15. Deng, Q.; Liu, Y.; Ci, L. A multi-magnet vibration energy harvester using ferromagnetic yokes to increase the power density. *Appl. Energy* **2017**, *208*, 1246–1253.
16. Xie, L.; Cai, Y.; Dai, Q. A segmented magnet design for improved performance of linear electromagnetic vibration energy harvester. *Mech. Syst. Signal Process*. **2019**, *127*, 523–537.
17. Zhou, S.; Cao, J.; Erturk, A.; Lin, J. Enhanced broadband piezoelectric energy harvesting using rotatable magnets. *Appl. Phys. Lett.* **2013**, *102*, 173901.
18. Toluwaloju, T.I.; Thein, C.K.; Halim, D. Flux feedback mechanism for realizing enhanced flux density in an electromagnetic vibration energy harvester. In Proceedings of the 2023 3rd International Conference on Electrical, Computer, Communications and Mechatronics Engineering (ICECCME), Tenerife, Canary Islands, Spain, 19–21 July 2023; pp. 1–6.
19. Peng, W.; Ni, Q.; Zhu, R.; Fu, X.; Zhu, X.; Zhang, C.; Liao, L. Triboelectric-electromagnetic hybrid wind energy harvesting and multifunctional sensing device for self-powered smart agricultural monitoring. *Nano Energy* **2024**, *131*, 110272.